3-1-2006

# Allele-specific deposition of macroH2A1 in imprinting control regions

Jung Ha Choo
*Louisiana State University*

Jeong Do Kim
*Louisiana State University*

Jae Hoon Chung
*Korea Advanced Institute of Science & Technology*

Lisa Stubbs
*Lawrence Livermore National Laboratory*

Joomyeong Kim
*Louisiana State University*



## Recommended Citation

Choo, J., Kim, J., Chung, J., Stubbs, L., & Kim, J. (2006). Allele-specific deposition of macroH2A1 in imprinting control regions. *Human Molecular Genetics, 15* (5), 717-724. https://doi.org/10.1093/hmg/ddi485

*Human Molecular Genetics, 2006, Vol. 15, No. 5* ***717–724***
*doi:10.1093/hmg/ddi485*
*Advance Access published on January 18, 2006*

# Allele-specific deposition of macroH2A1 in imprinting control regions

**Jung Ha Choo[1,2], Jeong Do Kim[1], Jae Hoon Chung[2], Lisa Stubbs[3] and Joomyeong Kim[1,*]**

[1]Department of Biological Sciences, Center for BioModular Multi-scale Systems, Louisiana State University, Baton Rouge, LA 70803, USA, [2]Department of Biological Sciences, Korea Advanced Institute of Science and Technology, Daejeon 305-701, South Korea and [3]Genome Biology Division, Lawrence Livermore National Laboratory, Livermore, CA 94551, USA

Received November 22, 2005; Revised and Accepted January 12, 2006

**In the current study, we analyzed the deposition patterns of macroH2A1 at a number of different genomic loci located in X chromosome and autosomes. MacroH2A1 is preferentially deposited at methylated CpG-rich regions located close to promoters. The macroH2A1 deposition patterns at the methylated CpG islands of several imprinted domains, including the imprinting control regions (ICRs) of Xist, Peg3, H19/Igf2, Gtl2/Dlk1 and Gnas domains, show consistent allele-specificity towards inactive, methylated alleles. The macroH2A1 deposition levels at the ICRs and other differentially methylated regions of these domains are also either higher or comparable to those observed at the inactive X chromosome of female mammals. Overall, our results indicate that besides DNA methylation macroH2A1 is another epigenetic component in the chromatin of ICRs displaying differential association with two parental alleles.**

## INTRODUCTION

The nucleosome is the basic unit of eukaryotic chromatins that consists of 146 bp DNA wrapped around a histone octamer composed of two copies of the canonical core histones, H2A, H2B, H3 and H4. Actively transcribed genes are associated with decondensed chromatin structure often illustrated by a 'beads-on-a-string' model, whereas silenced genes are associated with closed chromatin structure involving the linker histone H1, which is described as a '30 nm chromatin fiber.' These different chromatin structures are managed by several different strategies in eukaryotes, including chromatin remodeling, covalent modification on the N-terminal tails of histones and replacing canonical core histones with other variant forms. The core histones H3 and H2A have several variant forms that are conserved from yeast to humans. CENP-A is a variant form of H3 that is usually localized in constitutive heterochromatic regions, the centromeric regions of chromosomes, whereas macroH2A, the variant form of H2A, is localized in the facultative heterochromatin region, such as the inactive X chromosome of female mammals. The non-random distribution of these histone variants reflects the specialized roles of these variants in the formation of heterochromatin structure in chromosomes (1).

In contrast to other canonical and variant forms of histones, macroH2A has an unusual protein structure, and the size of this protein is three times that of the canonical counterpart, H2A. The N-terminal third of macroH2A (H2A-like) shares 64% sequence identity with H2A, and the remaining two-thirds of the protein show similarity with the domain called 'macro' (2). MacroH2A is conserved throughout all vertebrate lineages, and two different members of the macroH2A family have been identified so far, including macroH2A1 and macroH2A2 (3,4). Recent crystallographic studies suggest that the macro domain of macroH2A1 has the capability to bind to 2′- or 3′-*O*-acetyl-ADP-ribose (OAADPR), which is a well-known metabolite derived from the protein deacetylation reaction by sirtuins (orthologs of the yeast silent information regulator 2, SIR2) (5). The macro domain itself is shown to have transcriptional repression activity when fused to the DNA-binding domain of the yeast Gal4 (6), and the macroH2A-containing nucleosomes are also refractory to the chromatin remodeling complex SWI/SNF as well as the transcription factor NF-κB (7). Consistently, macroH2A is found to be highly concentrated in the inactive X chromosome of female mammals, which undergoes a chromosome-wide repression to balance the different dosage of X chromosome genes between male and female mammals (8,9).

*To whom correspondence should be addressed. Tel: +1 2255787692; Fax: +1 2255782597; Email: jkim@lsu.edu

A subset of autosomal genes in mammals are also subject to a similar dosage control, genomic imprinting, by which one of two parental alleles of these genes is repressed in a parental-origin-specific manner. These imprinted genes are clustered in specific regions of chromosomes, which has been an indication that the imprinting of a given domain is regulated by long-range controlling mechanisms. The imprinted genes are usually associated with CpG-rich regions nearby their promoters showing differential methylation between two parental alleles. Some of these differentially methylated regions (DMRs) function as imprinting control regions (ICRs), and deletions of these ICRs disturb the transcription and imprinting (allele-specific expression) of nearby genes that are sometimes located at million base pair genomic distances (10,11). Although the mechanism by which these ICRs control other genes' imprinting is currently investigated vigorously by a number of groups, little is known about the basic molecular features of these ICRs except for differential methylation and frequent association of ICRs with the mammalian insulator CTCF (12,13). Genomic imprinting also shares many similarities with the X chromosomal inactivation in terms of epigenetic inheritance patterns and evolutionary origin, and thus these two phenomena are postulated to share molecular machineries for gene repression (14–16).

The molecular basis for macroH2A targeting to the inactive X is still largely unknown, except for the fact that the H2A-like domain of macroH2A is responsible for this targeting (17). In order to provide insights regarding this mechanism, we analyzed the distribution patterns of macroH2A1 at a number of genomic loci located in X chromosome and autosomes with detailed chromatin immunoprecipitation (ChIP) assays. Our results indicated that methylated CpG islands are the prime targets for macroH2A1 deposition. During the course of this study, we also discovered that macroH2A1 is highly enriched in the inactive allele of ICRs in an allele-specific manner. This allele-specific deposition pattern of macroH2A1 in ICRs provides new hints regarding how the ICRs may control genomic imprinting in a chromatin environment.

## RESULTS

### MacroH2A1 localization to the inactive Xist locus of male X chromosome

To examine the distribution patterns of macroH2A1, we analyzed several genomic loci located in the X chromosome. For these experiments, we used mouse brain tissues derived from neonatal female (F1) and male (F2) hybrids that were generated through interspecific crossing of *Mus musculus* (C3H) and *M. spretus* (Fig. 1B). Homogenized tissues were treated with formaldehyde for cross-linking and immunoprecipitated with anti-macroH2A1 polyclonal antibodies. The precipitated DNAs were used for the PCR analysis of the following three loci. The first locus (primer set 5 of Xist) is a small CpG island located 1 kb downstream of the Xist transcription start site, and this region also contains alternative transcription start site for Xist (Fig. 1A). The other two loci are the promoter regions of X-linked genes, Hcfc1 (host cell factor C1) and AK122447, respectively (Fig. 1B). As expected, the enrichment of macroH2A1 for the two loci, Hcfc1 and AK122447, is detected only in female but not in male, consistent with the previous observation that macroH2A1 is localized mainly in the inactive X of female. However, the enrichment of macroH2A1 for the Xist locus was detected not only in female but also in male, and furthermore the enrichment levels were consistently similar between male and female tissues (Fig. 1B and C). The detection of macroH2A1 enrichment in male X was unexpected, which subsequently hinted us that macroH2A1 deposition at the Xist locus of male X is caused by or reflects the inactive state of this locus in male X. The Xist locus is inactivated in the active X that is shared by both sexes, whereas the Xist locus is active in the inactive X that is present only in female (Fig. 1D). Therefore, the detection of similar levels of macroH2A1 enrichment at the Xist locus between male and female suggests that the immunoprecipitated DNA at the Xist locus of female may be originated from the active X rather than the inactive X. This also implies that macroH2A1 is deposited to the Xist locus in an opposite manner relative to the rest of X-linked genes and also in a reciprocal manner between the two X chromosomes of female (Fig. 1D).

To further confirm this initial observation, we performed more analyses of macroH2A1 distribution using 10 different primer sets covering the 50 kb Xist/Tsix genomic interval (Fig. 1A and C). The Xist locus of male X also appears to be a good target region to study the distribution patterns of macroH2A1 mainly because the haploid state of male X is expected to derive more unequivocal results than other chromosomes with diploid state. An equal amount (0.1 g) of mouse brain tissues was used for each of three independent ChIP experiments followed by quantitative PCR analyses. The fixed amount (16 ng = 4000 genome equivalents) of mouse genomic DNAs was used as a reference to derive the relative enrichment level for a given region (Fig. 1C). Three different regions showed relatively high levels of macroH2A1 enrichment. Primer set 5 showed the highest enrichment with the averaged value being 0.4 (1600 copies), and the other two regions, primer sets 3 and 9, showed 0.17 and 0.23, respectively. The remaining seven regions showed much lower levels, ranging from 0 to 0.1. A similar pattern was also observed from the Xist locus of female X (Fig. 1C). The reason for the higher levels of macroH2A1 enrichment at these three regions is currently unknown, but our careful inspections revealed the following shared features at these regions. All three regions are located either within or nearby the promoters of the Xist/Tsix locus. Primer sets 3 and 5 are located within the first and second promoter regions of Xist, whereas primer set 9 is nearby the second promoter of Tsix. All three regions are also part of CpG islands, and furthermore two regions, primer sets 3 and 5, are known to be methylated in male X (18). This suggests a potential link between macroH2A1 deposition and CpG methylation.

### MacroH2A1 deposition in the methylated allele of Peg3-DMR

Because of the initial observation, preferential deposition of macroH2A1 in methylated CpG islands, we further analyzed the macroH2A1 distribution patterns in several well-known

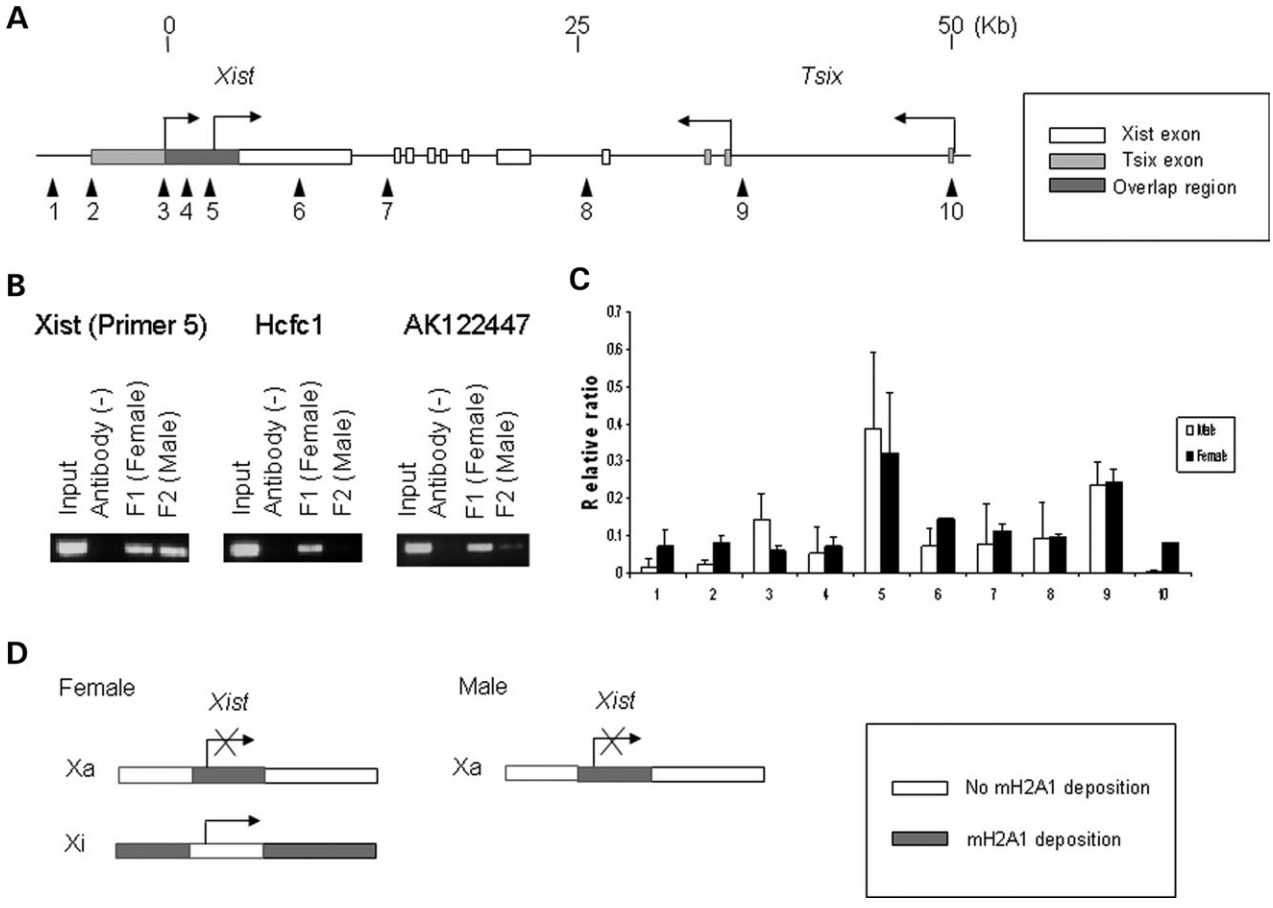


**Figure 1.** MacroH2A1 deposition on the male Xist locus. (**A**) The genomic structure of *Xist*. The arrows indicate the direction of Xist and Tsix transcription, and each gene has two different transcription start sites. The arrowheads with numbers represent the primer positions used for the quantitative PCR analyses of macroH2A1 deposition levels. (**B**) ChIP with anti-macroH2A1 antibody. Two mouse brain tissues from female (F1, lane 3) and male (F2, lane 4) were used for our ChIP analyses. These ChIP analyses also included two control DNAs: input DNAs (lane 1) and the precipitated DNAs without the anti-macroH2A1 antibody (lane 2). These DNAs were used as templates for the PCR amplification of Xist, Hcfc1 and AK12447 promoter regions, which are all located in the X chromosome. (**C**) Profiling of macroH2A1 deposition on the Xist locus of male and female. The immunoprecipitated DNAs were analyzed with quantitative PCR using the 10 primer sets targeting the Xist locus, the positions of which are shown in (A). The graph shows the averaged enrichment levels with the standard errors that were calculated from three independent ChIP experiments. Each primer set used 1 μl of the ChIP DNA that has been prepared from 0.1 g of mouse brain and subsequently dissolved in the total 40 μl volume. The amplification of each primer set was further calculated with the fixed amount of genomic DNAs (16 ng) to derive the relative ratio for a given primer set, the value shown on the *Y*-axis. (**D**) Schematic representation of macroH2A1 deposition patterns on X chromosome. This is based on the interpretation of the results shown in (B), the macroH2A1 deposition patterns of three X-linked genes. MacroH2A1 is deposited on the inactive Xist locus of active X chromosome present in both male and female. Meanwhile, in the other two loci, Hcfc1 and AK122447, macroH2A1 was accumulated only on the inactive X present in female.

imprinted domains that have methylated CpG islands. First, we targeted the Peg3-imprinted domain located in the proximal region of mouse chromosome 7 (Fig. 2A). This 500 kb domain contains three paternally expressed genes, Peg3, Usp29 and Zfp264, and three maternally expressed genes, Zim1, Zim2 and Zim3/Usp29as (19). This domain also contains one non-imprinted gene, Stk13 (Ser/Thr kinase 13), which is expressed only in adult-stage testis. The promoters of all these genes except for Stk13 are associated with CpG-rich regions, and most of these CpG islands are not methylated on both alleles (J. Kim, unpublished data). However, the 5 kb CpG island encompassing the bidirectional promoter of Peg3/Usp29 is methylated in an allele-specific manner: only the maternal allele of this region is methylated, hence referred to as Peg3-DMR (20). We surveyed the macroH2A1 distribution within this domain using 19 primer sets targeting the promoters, exons, introns and 3′-UTRs of resident genes (Fig. 2A). Out of 19 primer sets, the two regions located within the Peg3-DMR, the promoter region of Peg3/Usp29 (primer set 13) and the first intron of Peg3 (primer set 14), showed the highest levels of macroH2A1 enrichment. To quantify the relative ratios of the enrichment levels among different regions, we performed quantitative PCR analyses using the primer sets amplifying the promoter regions of this domain (Fig. 2B). The Xist locus (primer set 5 in Fig. 1) was used as an independent internal control. The two regions located within the Peg3-DMR showed 1.5- to 2-fold more enrichment than the internal control Xist locus, whereas the macroH2A1 enrichment levels were much lower at the three other promoter regions, including 0.4-fold at Stk13 (primer set 1), 0.5-fold at Zfp264/Zim3 (primer set 2) and 0.3-fold at Zim1 (primer set 16). The value for the

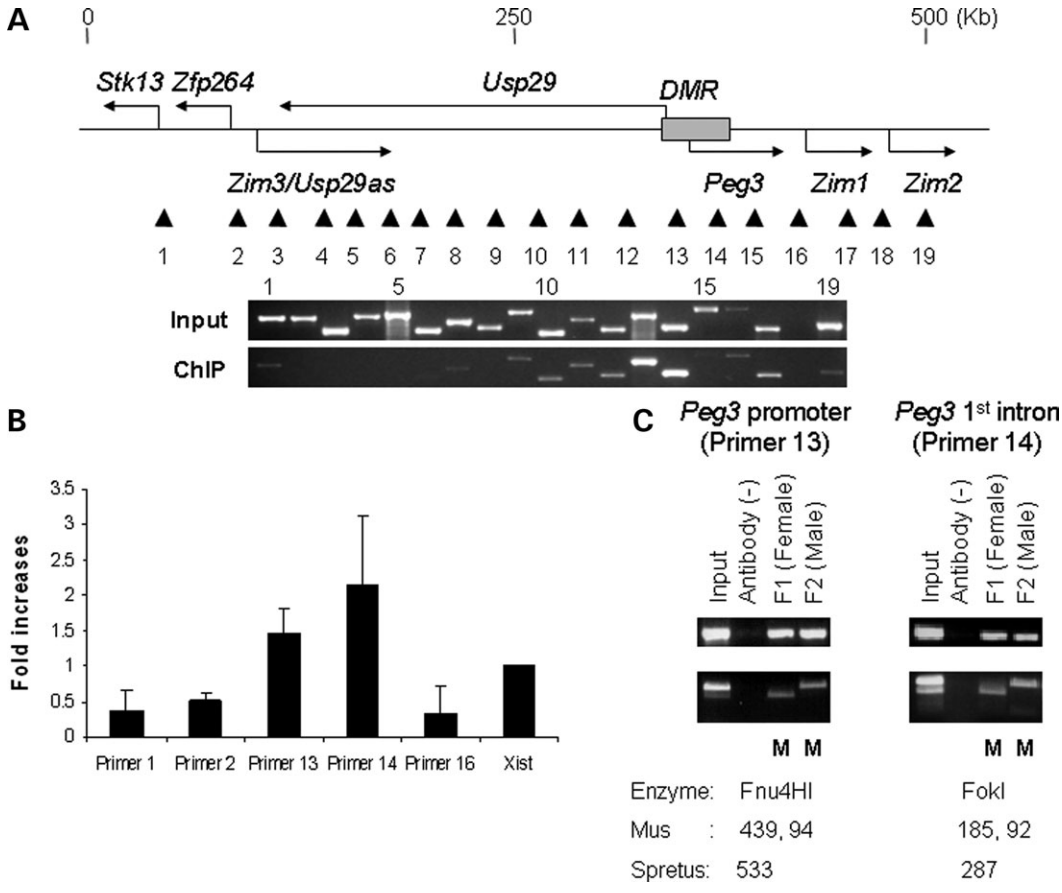


**Figure 2.** MacroH2A1 deposition on the Peg3 imprinted domain. (**A**) The genomic organization of the mouse Peg3 domain. The arrows indicate the transcriptional direction of imprinted genes. The filled box represents the Peg3-DMR. The arrowheads with numbers represent the positions of the 19 primer sets amplifying the promoter, exon, intron, 3′-UTR regions of resident genes. The input and immunoprecipitated DNAs were used as templates for the PCR amplification using the 19 primer sets. (**B**) Quantitative PCR analysis of macroH2A1 deposition. The deposition level of macroH2A1 at the promoter regions of the Peg3-domain was presented as fold increase relative to the level at the Xist locus (primer set 5 of Fig. 1). The values on the *Y*-axis represent the average fold increases with standard errors that were calculated from three independent ChIP experiments. (**C**) Determination of the allelic origin of immunoprecipitated DNAs. The macroH2A1-immunoprecipitated DNAs at primer sets 13 and 14 were further analyzed in terms of their parental origins. This analysis utilized sequence polymorphisms detected between the two parental species of our hybrid mice, F1 and F2. In F1 mice (lane 3), the paternal allele is from *M. spretus* and the maternal from *M. musculus*, which was switched in F2 mice (lane 4). Two separate restriction enzyme digestions on the promoter (primer set 13) and first intron (primer set 14) regions of Peg3 clearly demonstrated the presence of two parental alleles in the input DNAs (lane 1). However, the macroH2A1-immunoprecipitated DNAs at both regions were mainly derived from the maternal allele. M stands for the maternal allele.

Zim2 promoter is not available due to technical difficulties stemming from spurious PCR reactions (primer set 18). The Peg3-DMR is the only CpG island that is methylated within the Peg3-imprinted domain, and therefore the high levels of macroH2A1 enrichment at the Peg3-DMR is consistent with the initial observation derived from the Xist locus showing preferential deposition at methylated CpG islands.

To confirm further whether macroH2A1 is deposited only to the methylated allele of the Peg3-DMR, we analyzed the allelic origin of the macroH2A1-immunoprecipitated DNAs at the two regions, primer sets 13 and 14 (Fig. 2C). Sequence polymorphisms within each of these two regions were identified and used to differentiate the two parental alleles of the F1 and F2 hybrid mice. Two separate restriction enzyme digestions designed to detect the sequence polymorphisms clearly demonstrated that the immunoprecipitated DNAs at these two regions were derived mainly from the methylated, maternal allele of the Peg3-DMR. This test confirms again that methylated CpG islands are prime targets for macroH2A1 deposition. It is worthwhile to point out the deposition level at the promoter of Stk13 (primer set 1). In contrast to the other genes in the Peg3-imprinted domain, this testis-specific gene is completely inactive in the brain tissue, which was used for our ChIP experiments. The promoter of this gene is also not associated with any CpG island. Therefore, the low level of macroH2A1 deposition at the Stk13 locus further suggests that methylation on CpG islands, but not simply the inactive state of a locus, coincides with macroH2A1 deposition.

### Allele-specific deposition of macroH2A1 in other ICRs

We also examined the deposition patterns of macroH2A1 at three other imprinted domains, including H19/Igf2, Gtl2/Dlk1 and Gnas domains, and the results of H19/Igf2 and Gtl2/Dlk1 domains are shown in Figures 3 and 4, respectively.

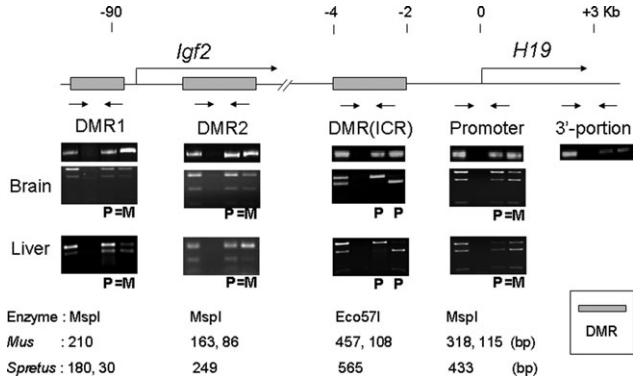


**Figure 3.** Allele-specific deposition of macroH2A1 at the H19/Igf2 ICR. Shown is the genomic structure of H19/Igf2 imprinted domain. The arrows indicate the transcriptional directions of genes and the regions marked by gray boxes are DMRs. The pairs of arrowheads underneath the genomic structure indicate the positions of primer sets for the PCR amplification of ChIP DNAs. The amplified PCR products of each region are shown as the same order as previous figures: input (lane 1), the ChIP DNA without macroH2A1 antibody (lane 2), the ChIP DNA from F1 (lane 3) and F2 (lane 4). Each PCR product was further digested with a proper restriction enzyme to determine the parental origin of each immunoprecipitated DNA. The used restriction enzymes and estimated sizes of digested PCR products are shown below. In F1 mice (lane 3), the paternal allele is from *M. spretus* and the maternal allele is from *M. musculus*. In F2 mice (lane 4), two species alleles were switched reciprocally in terms of their parental origins. At the DMR/ICR of the H19/Igf2-imprinted domain, macroH2A1 is mainly deposited at the methylated, paternal allele.

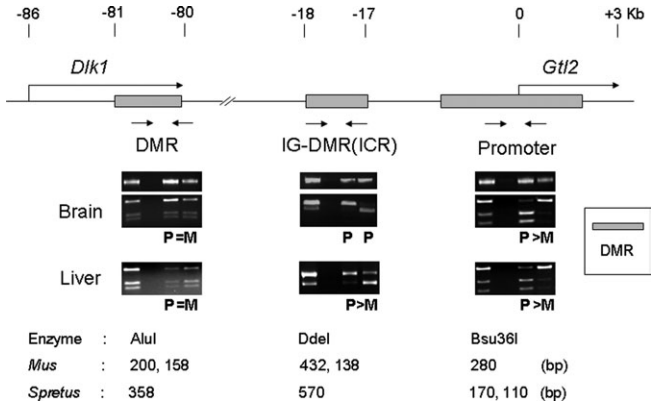


**Figure 4.** Allele-specific deposition of macroH2A1 at the Gtl2/Dlk1 ICR. Shown is the genomic structure of Gtl2/Dlk1 imprinted domain. The arrows indicate the transcriptional directions of genes and the regions marked by gray boxes are DMRs. The pairs of arrowheads underneath the genomic structure indicate the positions of primer sets for the PCR amplification of ChIP DNAs. The amplified PCR products of each region are shown as the same order as previous figures: input (lane 1), the ChIP DNA without macroH2A1 antibody (lane 2), the ChIP DNA from F1 (lane 3) and F2 (lane 4). Similar to Figure 3, each PCR product was also digested with a proper restriction enzyme and the different sizes of the digested products with each restriction enzyme are shown below. The IG-DMR also shows a similar result as the H19/Igf2 domain, methylated paternal allele-specific deposition of macroH2A1.

For these experiments, we used brain and liver tissues prepared from neonatal and adult mice. The data sets shown in Figures 3 and 4 were derived from the tissues of neonatal mice. For the H19/Igf2-imprinted domain, we targeted five regions, including the two DMRs of Igf2, the H19-DMR with an imprinting controlling activity, the H19 promoter region and the 3′-portion of H19 (21). The relatively high levels of macroH2A1 enrichment were detected at the DMRs of Igf2 and H19 as well as the promoter region of H19. In contrast, much lower levels were observed at the 3′-portion of H19. With the same strategy described for the Peg3 domain, the immunoprecipitated DNAs at these regions were further analyzed in terms of their parental origins. The DNAs at the two DMRs of Igf2 were derived equally from both alleles in the brain and liver of both neonatal and adult mice. This is somewhat consistent with the methylation status of these two DMRs in the tissues we tested. The differential methylation patterns of Igf2-DMR1 and Igf2-DMR2 are highly mosaic and tissue-specific. In particular, the Igf2-DMR2 is differentially methylated in fetal liver, but not in the brain and liver of neonatal and adult mice (22). In contrast, the DNAs at the H19-DMR were derived mainly from the methylated allele of H19, paternal allele. This allele-specific deposition pattern of macroH2A1 at the H19-DMR was also observed consistently in the tissues of the adult mice (data not shown). This agrees very well with the stable methylation status of this DMR in different tissues as well as in different developmental stages (23).

For the Gtl2-imprinted domain, we mainly analyzed three DMRs: the DMR of Dlk1 located in the surrounding regions of fifth exon, the IG-DMR (Intergenic DMR; 17 kb upstream of Gtl2) that has been shown to be an ICR for this domain (24) and the promoter region of Gtl2 located within another DMR (25). The overall enrichment levels at these three regions were similar to each other (Fig. 4). Our subsequent allele tests of these regions showed that the immunoprecipitated DNAs at IG-DMR were mainly derived from the methylated, paternal allele in both brain and liver of neonatal mice. The promoter region also showed allele bias toward to the methylated, paternal allele, but with much less obvious than IG-DMR. However, the DNAs at the DMR located nearby the fifth exon of Dlk1 were derived equally from both parental alleles. The similar deposition patterns of macroH2A1 at the Gtl2/Dlk1 domain were also observed in the brain and liver of the adult mice (data not shown). As seen in the H19/Igf2 domain, the different levels of allele specificity observed among the three DMRs of the Gtl2/Dlk1 domain are also consistent with the different methylation status of these DMRs among tissues. The differential methylation patterns on the promoter region of Gtl2 and the Dlk1-DMR are also mosaic and tissues-specific (25). In contrast, the methylation status of the IG-DMR is consistent and stable throughout development and also inherited as a gametic signal as seen in the H19-DMR.

Our analyses on the third imprinted domain, the Gnas domain, also derived a similar result, preferential and methylated-allele biased deposition of macroH2A1 at the DMR located nearby the promoter region of Nespas, which is also an ICR for this domain (data not shown) (26). Overall, our series of ChIP experiments derived a consistent result that macroH2A1 is deposited preferentially at the DMRs of imprinted domains. It is also interesting to note that macroH2A1 shows much clear allele-specific deposition pattern at the ICRs of all the domains tested. This allele-specific

deposition pattern of macroH2A1 parallels very well with the differential methylation pattern of these ICRs.

### Relative ratios of macroH2A1 deposition levels among different loci

We also performed a series of quantitative measurement of the macroH2A1 deposition levels at different genomic regions (Fig. 5). For these analyses, both female and male brain tissues were analyzed separately with the Xist locus as an internal control. We included six autosomal genes, AK007485, Nr3c1 (glucocorticoid receptor), Myc, Ptbp1 (Polypyrimidine tract-binding protein 1), Sp1 and Pro, which are expressed ubiquitously in all tissues. MacroH2A1 deposition levels at these six loci were very minimal in both female and male tissues, as the enrichment levels of these loci were only about one-fourth the level at Xist. Similar levels of macroH2A1 deposition were detected in all X-linked genes in male, including Hcfc1 (0.13-fold), Tsix (antisense of Xist) and AK122447. In female tissues, however, all these X-linked genes showed the enrichment levels comparable to the Xist locus as shown in the Hcfc1 locus (0.98-fold). In contrast to these X-linked genes, the enrichment levels at the DMRs/ICRs of imprinted domains were usually much higher, ranging from 1.2-fold at the H19-DMR to 3.2-fold at the first intron of Peg3 in the Peg3-DMR. These higher enrichment levels were also observed consistently in both brain and liver of neonatal and adult mice. More extended quantitative analyses of macroH2A1 deposition levels at the DMRs of imprinted domains are presented in Supplementary Material, Fig. S1. Overall, the macroH2A1 enrichment levels at the methylated alleles of DMRs were generally higher than those of X-linked genes in female, and it would be interesting to study in the near future what causes the different levels of macroH2A1 deposition among these different loci.

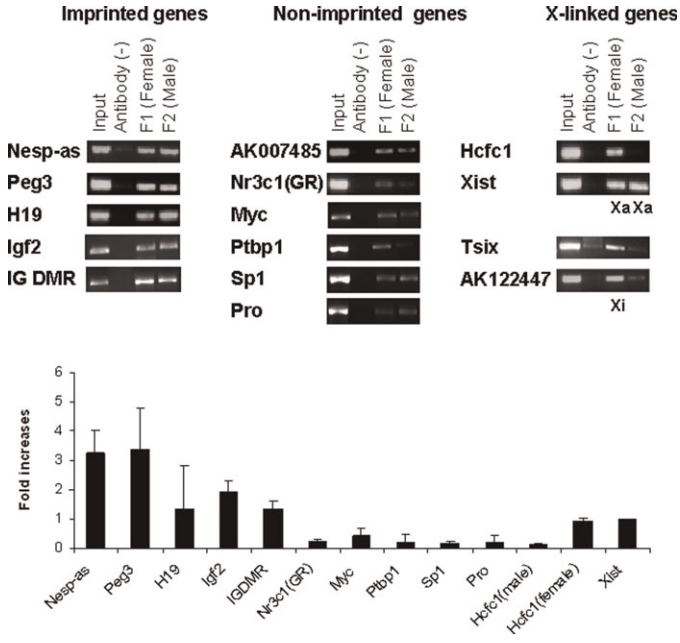


**Figure 5.** Relative ratios of macroH2A1 deposition among different loci. The deposition levels of macroH2A1 at different gene loci were analyzed and compared with quantitative PCR. The top panel shows the names of three groups of genes used for this survey. The amplified PCR products for each gene locus are shown in the same format as previous figures. The graph shown in the bottom summarizes the results of the quantitative PCR assays indicating the relative enrichment level of each locus compared with the Xist locus. The average fold increases with standard errors were calculated from at least three independent trials of the entire ChIP experiments. This quantitative analysis used female and male brains separately, and subsequently two values are shown in the case of X-linked genes, such as Hcfc1.

## DISCUSSION

In the current study, we presented for the first time the detailed deposition patterns of macroH2A1 at a number of different genomic loci. Our results indicated that macroH2A1 is preferentially deposited at methylated CpG-rich regions. The macroH2A1 deposition patterns at the ICRs of Xist, Peg3, H19/Igf2, Gtl2/Dlk1 and Gnas domains show consistent allele specificity towards inactive alleles, and also the macroH2A1 deposition levels at these ICRs and other DMRs are comparable to those of inactive X chromosomes. The allele-specific deposition pattern of macroH2A1 at these ICRs is reminiscent of the differential methylation pattern observed from these regions.

According to our results, macroH2A1 is highly enriched in the inactive alleles of ICRs that are heavily methylated. It is currently unknown how macroH2A1 is targeted to some heterochromatic regions, but the high levels of macroH2A1 enrichment at methylated CpG islands suggest that the targeting mechanism for macroH2A1 is closely linked to that of DNA methylation. This is also supported by several lines of evidence. First, during the initiation period of X chromosomal inactivation in embryonic stem (ES) cells, the macroH2A1 deposition occurs before DNA methylation, suggesting a potential sequential linkage of the two mechanisms, macroH2A1 deposition followed by DNA methylation (15). Secondly, another recent study using DNMT1-knockout ES cells demonstrated that loss of DNA methylation triggers the global reorganization involving macroH2A1 in constitutive heterochromatin regions, such as the centromeric regions of chromosomes. These regions are usually characterized by heavy DNA methylation and CENP-A localization, but not by macroH2A1 deposition (27). In this case, the relocalization of macroH2A1 is believed to function as a default, compensating mechanism for the maintenance of inactive state of de-methylated heterochromatic regions. This suggests that macroH2A1 deposition and DNA methylation may be two cooperating mechanisms for the maintenance of heterochromatic regions. It is also worthwhile to note the recent studies suggesting that histone methylation at Lys 9 and 27 of H3 may be involved in maintaining the repressive state of imprinted domains as a separate mechanism different from DNA methylation (28,29). Therefore, our detection of macroH2A1 deposition in the ICRs along with the results described above suggests one intriguing possibility that mammalian genomic imprinting may be regulated by at least three different, but cooperating, epigenetic mechanisms, DNA methylation, histone methylation and macroH2A1 deposition.

Allele-specific localization of macroH2A1 in ICRs provides a new hint regarding how the ICRs regulate the transcription of imprinted genes. Our data indicate that the deposition patterns at ICRs show very clear allele specificity: macroH2A1 is enriched at the inactive allele of ICRs, whereas excluded completely from the active alleles of ICRs. MacroH2A1-containing nucleosomes have been shown to be inaccessible to the nucleosome remodeling complex SWI/SNF as well as the transcription factors NF-κB (7). This inaccessibility is believed to be caused by the unusual chromatin structure stemming from the bulky macro domain. This macroH2A1-containing chromatin also appears to have the similar levels of compaction as H1-containing chromatins, suggesting that macroH2A1 may repress the transcription of nearby genes by forming highly compacted chromatin structure (30). In the case of the ICRs located nearby the promoters, such as Peg3, H19 and Gnas, the compact structure of chromatins driven by macroH2A1 provides a plausible mechanism for how ICRs might repress the nearby imprinted genes. The same study also hinted one possibility that macroH2A1 and H1 may be deposited in different chromatins in a mutually exclusive manner, implicating the presence of two distinct types of chromatin: the H1-containing chromatin and the macroH2A-containing, but H1-depleted, chromatin. It will be interesting to test whether the chromatins in the ICRs are mainly formed by macroH2A1-containing nucleosomes without H1.

A series of recent studies provide evidence pertinent to the potential function of the macro domain (5,31). According to X-ray crystallographic studies, one of the splicing variants of macroH2A1, macroH2A1.1, has a binding capability for OAADPR, the well-known metabolite for SIRT1 (the human ortholog of the yeast silent information regulator 2). The SIRT1 protein is a unique protein deacetylase utilizing NAD (nicotinamide adenine dinucleotide) as a cofactor and also a well-characterized protein involved in heterochromatin formation as well as other important functions of cells, such as aging and genomic instability (32,33). It remains to be further studied whether the functions of two heterochromatin-related proteins, macroH2A1 and SIRT1, are linked together through the metabolite OAADPR, but it adds another dimension on the complex regulatory networks controlling mammalian genomic imprinting.

## MATERIALS AND METHODS

### ChIP assay

ChIPs were performed according to the protocol provided by Upstate Biotechnology (Upstate Biotech., NY, USA) with some modification as described previously (34). Briefly, we used mouse brain and liver tissues derived from F1 (C3H × *Mus spretus*) and F2 (F1 × C3H) hybrids with two different ages, 10 days and 6 weeks old. Each of these tissues (0.1 g per tissue) was homogenized in 10 ml PBS for ChIP assay. The samples were treated with formaldehyde to final concentration of 1% and incubated at 37°C for 10 min. Treated samples were sheared by sonication to derive DNA fragments averaging 500 bp in length. Sheared chromatins were immunoprecipitated with anti-macroH2A1 antibody (Catalogue No. 07-219; Upstate Biotech.). Specificity of this antibody for ChIP application was tested through analyzing immunoprecipitated protein complexes with protein staining and western blot analyses (Supplementary Material, Fig. S2). Precipitated DNA and protein complexes were reverse cross-linked and purified through phenol/chloroform extraction. Purified DNA was used as templates for PCR amplification. The oligonucleotide sequences used for this study can be available upon request. PCR reactions were carried out for 36 cycles using standard PCR conditions. The resulting PCR products were analyzed by running on 1.6% agarose gel and staining with ethidium bromide. To rule out any artifact caused by the experimental steps of ChIP, we have repeated a series of control ChIP and allele test experiments using anti-H3 polyclonal antibody (Catalogue No. sc-10809; SantaCruz Biotech., Santa Cruz, CA, USA), and these results are presented in Supplementary Material, Fig. S3.

### Quantitative real-time PCR and data analysis

Quantitative real-time PCR was performed with iQ SYBR green supermix (Bio-Rad Laboratories, CA, USA) using the icycler iQ$^{TM}$ multicolor real-time detection system (Bio-Rad Laboratories). All PCR were carried out for 40 cycles under the standard PCR conditions. We analyzed the results of quantitative real-time PCR based on the threshold cycle (Ct) value. Owing to the inconsistent and very low efficient cross-linking step of ChIP, which usually causes high levels of variation among different trials, we used a fixed amount of purified genomic DNA as a reference instead of using the ChIP input DNAs (Supplementary Material, Fig. S4). A ΔCt was calculated by subtracting the Ct value for the genomic DNA (16 ng) from the Ct value from immunoprecipitated samples. For the relative quantity of Xist loci, we calculated the ΔCt ratio relative to the ΔCt of the genomic DNA. For the other loci, we calculated the relative amount by using the 2-ΔΔCt method (35). ΔΔCt value was calculated by subtracting the ΔCt value for the promoter of Xist (the highest region of Xist loci) from the Ct value for the other genomic loci. Fold differences were determined by raising 2 to the ΔΔCt power. We performed the entire procedure of ChIP analyses, starting from immunoprecipitation to quantitative real-time PCR, at least three independent times and the fold differences were presented as average ± standard errors.

## SUPPLEMENTARY MATERIAL

Supplementary Material is available at HMG Online.

## ACKNOWLEDGEMENTS

We thank Dr David Donze for critical reading of our manuscript. J.H. Choo is supported by the BK21 fellowship from the Department of Education, South Korea. This research was supported by National Institutes of Health R01 GM66225, National Science Foundation EPS-0346411 and the State of Louisiana Board of Regents Support Fund (J.K.).

*Conflict of Interest statement*. None declared.

## REFERENCES


1. Wolffe, A.P. (1998) *Chromatin: Structure and Function*, 3rd edn. Academic Press, San Diego, California.
2. Pehrson, J.R. and Fuji, R.N. (1998) Evolutionary conservation of histone macroH2A subtypes and domains. *Nucleic Acids Res.*, **26**, 2837–2842.
3. Chadwick, B.P. and Willard, H.F. (2001) Histone H2A variants and the inactive X chromosome: identification of a second macroH2A variant. *Hum. Mol. Genet.*, **10**, 1101–1113.
4. Pehrson, J.R. and Fried, V.A. (1992) MacroH2A, a core histone containing a large nonhistone region. *Science*, **257**, 1398–1400.
5. Kustatscher, G., Hothorn, M., Pugieux, C., Scheffzek, K. and Ladurner, A.G. (2005) Splicing regulates NAD metabolite binding to histone macroH2A. *Nat. Struct. Mol. Biol.*, **12**, 624–625.
6. Perche, P.Y., Vourc'h, C., Konecny, L., Souchier, C., Robert-Nicoud, M., Dimitrov, S. and Khochbin, S. (2000) Higher concentrations of histone macroH2A in the Barr body are correlated with higher nucleosome density. *Curr. Biol.*, **10**, 1531–1534.
7. Angelov, D., Molla, A., Perche, P.Y., Hans, F., Cote, J., Khochbin, S., Bouvet, P. and Dimitrov, S. (2003) The histone variant macroH2A interferes with transcription factor binding and SWI/SNF nucleosome remodeling. *Mol. Cell*, **11**, 1033–1041.
8. Chadwick, B.P. and Willard, H.F. (2003) Chromatin of the Barr body: histone and non-histone proteins associated with or excluded from the inactive X chromosome. *Hum. Mol. Genet.*, **12**, 2167–2178.
9. Costanzi, C. and Pehrson, J.R. (1998) Histone macroH2A1 is concentrated in the inactive X chromosome of female mammals. *Nature*, **393**, 599–601.
10. Brannan, C.I. and Bartolomei, M.S. (1999) Mechanisms of genomic imprinting. *Curr. Opin. Genet. Dev.*, **9**, 164–170.
11. Spahn, L. and Barlow, D.P. (2003) An ICE pattern crystallizers. *Nat. Genet.*, **35**, 11–12.
12. Bell, A.C. and Felsenfeld, G. (2000) Methylation of a CTCF-dependent boundary controls imprinted expression of the *Igf2* gene. *Nature*, **405**, 482–485.
13. Hark, A.T., Schoenherr, C.J., Katz, D.J., Ingram, R.S., Levorse, J.M. and Tilghman, S.M. (2000) CTCF mediates methylation-sensitive enhancer-blocking activity at the *H19/Igf2* locus. *Nature*, **405**, 486–489.
14. Huynh, K.D. and Lee J.T. (2005) X-chromosome inactivation: a hypothesis linking ontogeny and phylogeny. *Nat. Rev. Genet.*, **6**, 410–418.
15. Ogawa, Y. and Lee, J.T. (2002) Antisense regulation in X inactivation and autosomal imprinting. *Cytogenet. Genome Res.*, **99**, 59–65.
16. Reik, W. and Lewis, A. (2005) Co-evolution of X-chromosome inactivation and imprinting in mammals. *Nat. Rev. Genet.*, **6**, 403–410.
17. Chadwick, B.P., Valley, C.M. and Willard, H.F. (2001) Histone variant macroH2A contains two distinct macrochromatin domains capable of directing macroH2A to the inactive X chromosome. *Nucleic Acids Res.*, **29**, 2699–2705.
18. McDonald, L.E., Paterson, C.A. and Kay, G.F. (1998) Bisulfite genomic sequencing-derived methylation profile of the *Xist* gene throughout early mouse development. *Genomics*, **54**, 379–386.
19. Kim, J. and Stubbs, L. (2005) Rapidly evolving imprinted loci. *Encyclopedia of Genetics, Genomics, Proteomics and Bioinformatics*. John Wiley Publishers, West Sussex, UK.
20. Li, L.L., Szeto, I.Y., Cattanach, B.M., Ishino, F. and Surani, M.A. (2000) Organization and parent-of-origin-specific methylation of imprinted *Peg3* gene on mouse proximal chromosome 7. *Genomics*, **63**, 333–340.
21. Thorvaldsen, J.L., Duran, K.L. and Bartolomei, M.S. (1998) Deletion of the *H19* differentially methylated domain results in loss of imprinted expression of *H19* and *Igf2*. *Genes Dev.*, **12**, 3693–3702.
22. Feil, R., Walter, J., Allen, N.D. and Reik, W. (1994) Developmental control of allelic methylation in the imprinted mouse *Igf2* and *H19* genes. *Development*, **120**, 2933–2943.
23. Tremblay, K.D., Duran, K.L. and Bartolomei, M.S. (1997) A 5′ 2-kilobase-pair region of the imprinted mouse *H19* gene exhibits exclusive paternal methylation throughout development. *Mol. Cell. Biol.*, **17**, 4322–4329.
24. Lin, S.P., Youngson, N., Takada, S., Seitz, H., Reik, W., Paulsen, M., Cavaille, J. and Ferguson-Smith, A.C. (2003) Asymmetric regulation of imprinting on the maternal and paternal chromosomes at the *Dlk1–Gtl2* imprinted cluster on mouse chromosome 12. *Nat. Genet.*, **35**, 97–102.
25. Takada, S., Paulsen, M., Tevendale, M., Tsai, C.-E., Kelsey, G., Cattanach, B. and Ferguson-Smith, A. (2002) Epigenetic analysis of the *Dlk1–Gtl2* imprinted domain on mouse chromosome 12: implications for the imprinting control from comparison with *Igf2–H19*. *Hum. Mol. Genet.*, **11**, 77–86.
26. Plagge, A., Gordon, E., Dean, W., Boiani, R., Cinti, S., Peters, J. and Kelsey, G. (2004) The imprinted signaling protein XL alpha s is required for postnatal adaptation to feeding. *Nat. Genet.*, **36**, 818–826.
27. Ma, Y., Jacobs, S.B., Jackson-Grusby, L., Mastrangelo, M.A., Torres-Betancourt, J.A., Jaenisch, R. and Rasmussen, T.P. (2005) DNA CpG hypomethylation induces heterochromatin reorganization involving the histone variant macroH2A. *J. Cell Sci.*, **118**, 1607–1616.
28. Umlauf, D., Goto, Y., Cao, R., Cerqueira, F., Wagschal, A., Zhang, Y. and Feil, R. (2004) Imprinting along the Kcnq1 domain on mouse chromosome 7 involves repressive histone methylation and recruitment of Polycomb group complexes. *Nat. Genet.*, **36**, 1296–1300.
29. Lewis, A., Mitsuya, K., Umlauf, D., Smith, P., Dean, W., Walter, J., Higgins, M., Feil, R. and Reik, W. (2004) Imprinting on distal chromosome 7 in the placenta involves repressive histone methylation independent of DNA methylation. *Nat. Genet.*, **36**, 1291–1295.
30. Abbott, D.W., Chadwick, B.P., Thambirajah, A.A. and Ausio, J. (2005) Beyond the Xi: macroH2A chromatin distribution and post-translational modification in an avian system. *J. Biol. Chem.*, **280**, 16437–16445.
31. Karras, G.I., Kustatscher, G., Buhecha, H.R., Allen, M.D., Pugieux, C., Sait, F., Bycroft, M. and Ladurner, A.G. (2005) The macro domain is an ADP-ribose binding module. *EMBO J.*, **24**, 1911–1920.
32. Bordone, L. and Guarente, L. (2005) Calorie restriction, SIRT1 and metabolism: understanding longevity. *Nat. Rev. Mol. Cell Biol.*, **6**, 298–305.
33. Guarente, L. and Picard, F. (2005) Calorie restriction—the SIR2 connection. *Cell*, **120**, 473–482.
34. Kim, J., Kollhoff, A., Bergmann, A. and Stubbs, L. (2003) Methylation-sensitive binding of transcription factor YY1 to an insulator sequence within the paternally expressed imprinted gene, *Peg3*. *Hum. Mol. Genet.*, **12**, 233–245.
35. Applied Biosystems. (1997) *Applied Biosystems Bulletin 2*. Applied Biosystems, Foster City, CA.